Karlsruhe Institute of Technology

Fakultät für Physik
Institut für Theorie der Kondensierten Materie

Another thesis on SNS junctions: numerical simulations and calculations

Master's Thesis

by

Umut Nefta Kanilmaz

Submission date: 25. February 2018

Advisor: PD Dr. Igor Gornyi
Co-Advisor: Prof. Dr. Alexander Mirlin

Ich erkläre hiermit, dass die Arbeit selbstständig angefertigt, alle benutzten Quellen und Hilfsmittel vollständig und genau angegeben und alles kenntlich gemacht wurde, das aus Arbeiten anderer unverändert oder mit Abänderungen entnommen ist.

Karlsruhe, den 23. Februar 2018

Umut Nefta Kanilmaz

Contents

1 Analytical Model

1.1 Foundation of the quasiclassical model

From section **??** it is known that Andreev reflection of electrons in a SNS junction leads to Andreev bound states within the junction. Each one of these bound states contributes to the total current through the junction. Essentially, a bound state can be expressed as a trajectory from one superconductor through the normal metal to the other superconductor. The superconducting current density is found through geometrical analysis of possible trajectories. The total current density is then found by adding up all these trajectories. The two dimensional junction (schematic

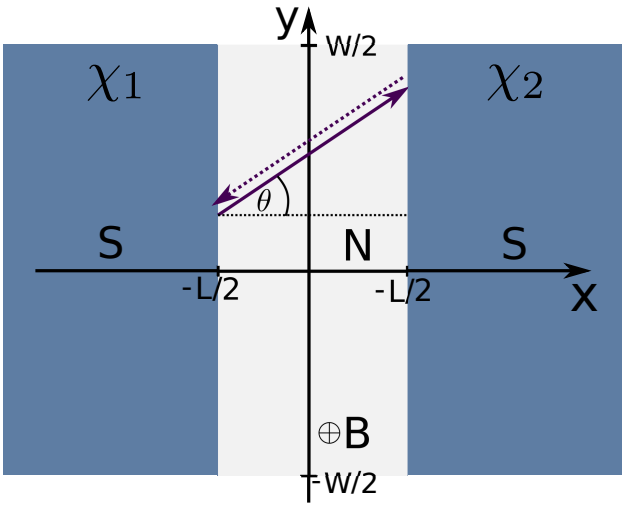

Figure 1.1: *SNS junction with width W and length L. A trajectory connecting the interfaces is parametrized by the angle θ between the trajectory and the x-axis. χ_1 and χ_2 are the superconducting phases, with total phase differece $\chi = \chi_2 - \chi_1$.*

shown in fig 1.1) is a short and wide junction with width W and length L, where $W \gg L$. The NS-interfaces are parallel to the y-axis and are placed at $x = \pm L/2$. Each of the superconducting leads has a phase χ_1 and χ_2, and the overall phase difference is $\chi = \chi_1 - \chi_2$. The superconducting gap parameter Δ is only present in the superconducting leads. Close to the interface, Δ begins to decay on a length scale of the superconducting coherence length ξ_0 into the normal region. Similar to the procedure in section **??**, this decay is neglected and a step-like behaviour is assumed for the superconducting gap parameter:

$$\Delta(x) = |\Delta| e^{\chi_1} \Theta\left(-L/2 - x\right) + |\Delta| e^{\chi_2} \Theta\left(x - L/2\right). \tag{1.1}$$

The thermal length scale of the system assumed to be larger than the sample length:

$$L_T = \hbar v_F / k_B T \gg L. \tag{1.2}$$

The transport through the junction is assumed to be ballistic, resulting in the trajectories being straight and not being altered by scattering in the normal region. However, the presence of the magnetic field in the normal region of the sample will lead to a bending of the trajectories due to the Lorentz force. Depending on the strength of magnetic field B and the Fermi velocity, the radius of this curve is

$$r_B = \frac{m v_F}{eB} \tag{1.3}$$

In order to justify the assumption of straight trajectories, either the magnetic field has to be weak enough, or the Fermi velocity (wavelength) has to be large (short) enough. Then, the cyclotron radius r_B is larger than the sample size L, and straight trajectories are a valid assumption.

1.2 Plane setup: calculation of current

Summing up the contributions leads to the current through the SNS junctions, the Josephson current $J\left(\chi\right)$, which is a function of the superconducting phase difference $\chi = \chi_2 - \chi_1$. By maximizing the Josephson current with respect to χ, one finds the critical current I_c.
A trajectory connecting the two superconducting interfaces can be parametrized by the angle θ between the trajectory and the x-axis. For a trajectory from a point $(-L/2, y_1)$ to another at $(+L/2, y_2)$, the angle for the parametrization is

$$\tan\theta = \frac{y_2 - y_1}{L}. \tag{1.4}$$

Figure 1.1 visualizes this parametrization. Several papers outline approaches to this problem ([**?**], [**?**]) and are based on the same concept. The Josephson current in [**?**] has the form

$$J = \frac{2e}{\pi L} \sum_{\boldsymbol{\kappa}} v_{Fx}^{\boldsymbol{\kappa}} \mathcal{J}\left(\chi\right), \tag{1.5}$$

where $\boldsymbol{\kappa}$ is the tangential momentum with $\boldsymbol{\kappa}^2 + \mathbf{k_x}^2 = k_F^2$. v_{Fx} is the projection of v_F on the x-axis

$$v_{Fx} = v_F \cos\theta \tag{1.6}$$

and $\mathcal{J}\left(\chi\right)$ is the current density. A similar ansatz to eq. (1.5) is described in [**?**]:

$$J = \int_{-W/2}^{+W/2} dy \int_{-p_F}^{+p_F} \frac{dp_y}{2\pi} \cos\theta \mathcal{J}\left(\chi, \phi\right). \tag{1.7}$$

For a fixed point at the left interface, the current density is integrated over all possible momenta. This integral can be expressed through the endpoints of a trajectory. The integration over p_y can then be replaced by $p_y = p_F \sin\theta \rightarrow dp_y/d\theta = p_F \cos\theta$. The integration over the angle θ can be substituted by the integration over y_2, a point at the right interface. The result for the Josephson current reads

$$J\left(\chi, \phi = 0\right) = \frac{2e v_F}{\pi \lambda_F L^2} \int \int_{-W/2}^{W/2} dy_1 dy_2 \frac{\mathcal{J}(\chi)}{\left[1 + \left(\frac{y_1 - y_2}{L}\right)^2\right]^2}. \tag{1.8}$$

By maximizing the Josephson current with respect to χ, the critical current can be found as:

$$I_c(\phi) = \max_\chi \left\{ J(\chi, \phi) \right\}. \tag{1.9}$$

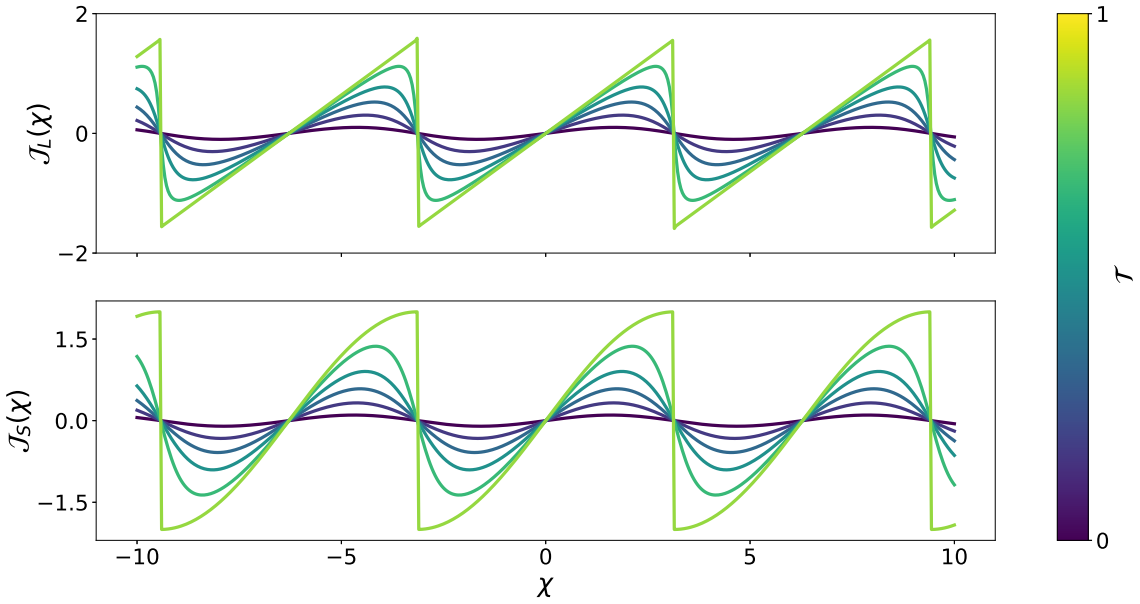

Figure 1.2: *Current density plotted against the superconducting phase difference $\chi = \chi_2 - \chi_1$. The density from eq. (1.11) gives the sawtooth like shape for $\mathcal{J}^l$ for high values of $\mathcal{T}$. In the short junction limit, $\mathcal{J}^s$ holds from eq. (1.10). For low values of the transmission coefficient $\mathcal{T}$, both current densities look similar (sinusoidal form).*

The current density $\mathcal{J}$ depends on the ratio of W and L. For $W \gg L$, the junction is a short junction, while for $W \ll L$, it is a long junction. In the short junction limit, the current density is calculated in [**?**]

$$\mathcal{J}^s(\chi) = \frac{\mathcal{T}_n \sin\chi}{\sqrt{1 - \mathcal{T}_n \sin^2\frac{\chi}{2}}} \tag{1.10}$$

which can be derived in the framework of the scattering matrix formalism. $\mathcal{T}_n$ is the transmission coefficient for a given conducting channel. For low transmission, $\mathcal{T} \ll 1$, only the first addend contributes, which leads to the conventional Josephson relation $J \simeq \mathcal{T} \sin\chi$.
For the long junction, from [**?**] the following expression can be found:

$$\mathcal{J}^l(\chi) = \sum_{k=1}^{\infty} \frac{(-1)^{k+1}\mathcal{T}^k}{k} \sin\big(k\chi\big). \tag{1.11}$$

The coefficient $\mathcal{T}$ has been included phenomenologically in this formula and includes the normal scattering in the sample. Figure 1.2 shows a plot of both short and long junction limit current densities. For $\mathcal{T} \ll 1$, $\mathcal{J}^s$ takes a sinusoidal form, which also true for the long junction limit. For each of those, the classical Josephson relation can be found in the limit of low transmissions:

$$\mathcal{J} \simeq \mathcal{T} \sin\chi \tag{1.12}$$

The current densities differ for a large transmission coefficient $\mathcal{T} \simeq 1$: A sawtooth-like shape is observed in the long junction limit, and in the short junction limit, a sinusoidal shape appears.

Including magnetic field

Up to this point, the current has been derived for zero magnetic field. If a finite magnetic field is considered, the phase χ is modified because of two effects: First, the magnetic phase that will be acquired along a trajectory connecting two points y_1 and y_2 leads to an additional term in the phase. Also, the superconducting phases at each interface become functions of $y_{1/2}$ (see [**?**]):

$$\begin{aligned} \chi_{1/2} &= \mp\frac{1}{2}\left(\chi - \frac{2\pi BL}{\phi_0} y_{1/2}\right) && (1.13)\\ \tilde{\chi}(y_1, y_2) &= \chi_2 - \chi_1 && (1.14)\\ &= \chi - \frac{\pi BL}{\phi_0}(y_1 + y_2) && (1.15) \end{aligned}$$

Assuming that the London penetration depth is small to zero in the superconducting regions, the following gauge for the vector potential can be used:

$$\mathbf{A} = A_y \mathbf{e}_y, \quad A_y = \begin{cases} -Bx, & -L/2 \le x \le L/2, \\ -\frac{1}{2}BL|x|, & |x| > L/2 \end{cases} \tag{1.16}$$

This gauge will give no additional contribution to the phase on straight trajectories

$$\begin{aligned} \delta\chi &= \frac{2\pi}{\Phi_0}\int d\mathbf{l}\cdot\mathbf{A} && (1.17)\\ &= \frac{2\pi}{\Phi_0}\int_{-L/2}^{L/2}\frac{dx}{\cos\theta} A_y(x)\sin\theta && (1.18)\\ &= -\frac{2\pi B}{\Phi_0}\frac{y_2 - y_1}{L}\int_{-L/2}^{L/2} x dx && (1.19)\\ &= 0, && (1.20) \end{aligned}$$

where eq. (1.4) has been used. The total phase for this setup is therefore eq. (1.15). This results in the current phase relation in the expression for the Josephson current from eq. (1.8) to be replaced by the effective phase $\chi \to \tilde{\chi}(y_1, y_2)$:

$$J\left(\chi, \phi\right) = \frac{2ev_F}{\pi\lambda_F L^2}\int\int_{-W/2}^{W/2} dy_1 dy_2 \frac{\mathcal{J}(\tilde{\chi}(y_1, y_2))}{\left[1 + \left(\frac{y_1 - y_2}{L}\right)^2\right]^2} \tag{1.21}$$

The critical current can be found by maximizing the Josephson current with respect to χ:

$$I_c(\phi) = \max_\chi \left\{J(\chi, \phi)\right\}. \tag{1.22}$$

The integation over y_1 and y_2 has been evaluated in **TODO cite!** yields the critical current

$$I_c(\chi) = \frac{2eWv_F}{\lambda_F L}\frac{(1 - \{\phi\})\{\phi\}}{|\phi|} \tag{1.23}$$

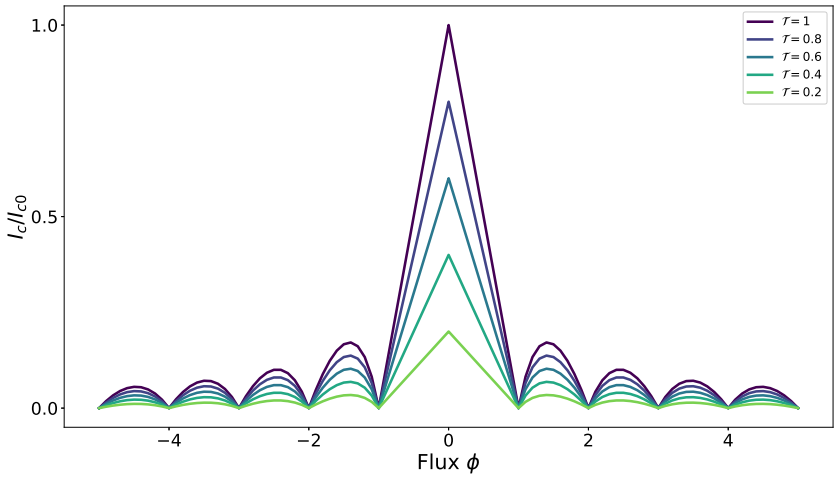

Figure 1.3: *I_c vs. ϕ for different values of $\mathcal{T}$*

Including scattering at the boundaries

So far, straight trajectories connecting the two superconducting interfaces have been considered. A process that is possible in principal, is a trajectory of an electron that is scattered at a side boundary (see figure **TODO!**). It is clear that, especially in the case of a short and wide junction with $W \gg L$, these trajectories do not contribute as much as the straight trajectories. When a trajectory is scattered at, say, a point at the upper edge $(x, y) = (x_s, pW/2)$, the parametrisation for the angle describing the trajectory is

$$\tan\theta = \frac{\bar{y}_2 - y_1}{L} = \frac{W - y_2 - y_1}{L}. \tag{1.24}$$

In this parametrisation, the coordinate $\bar{y}_2$ is the mirror image of y_2. For straight trajectories the vector potential $\mathbf{A}$ does not give an additional contribution, which can be seen in eq. (**??**). The effective phase is in this case determined by eq. (1.15). When considering the scattering at side boundaries with the parametrization from eq. (1.24), the contribution from the magnetic phase is no longer zero,

$$\begin{aligned}
\delta\chi &= \frac{2\pi}{\Phi_0}\int_{-L/2}^{x_s} dx A_y(x)\tan\theta - \frac{2\pi}{\Phi_0}\int_{x_s}^{+L/2} dx A_y(x)\tan\theta && (1.25)\\
&= -\frac{2\pi B}{\Phi_0}\tan\theta\left(\int_{-L/2}^{x_s} x dx - \int_{x_s}^{+L/2} dx\right) && (1.26)\\
&= -\frac{2\pi B}{\Phi_0}\tan\theta\left(x_s^2 - (L/2)^2\right) && (1.27)\\
&= \frac{\pi\phi}{2W}\frac{(W-2y_1)(W-2y_2)}{W-y_1-y_2}, && (1.28)
\end{aligned}$$

since the trajectory changes the direction and therefore $d\mathbf{l}\cdot\mathbf{A}$ changes sign. The total effective phase difference is then, using eq. (1.15)

$$c\tilde{h}i(y_1, y_2) = \chi - \frac{\pi\phi}{2W}\left(2(y_1+y_2) - \frac{(W-2y_1)(W-2y_2)}{W-y_1-y_2}\right) \tag{1.29}$$

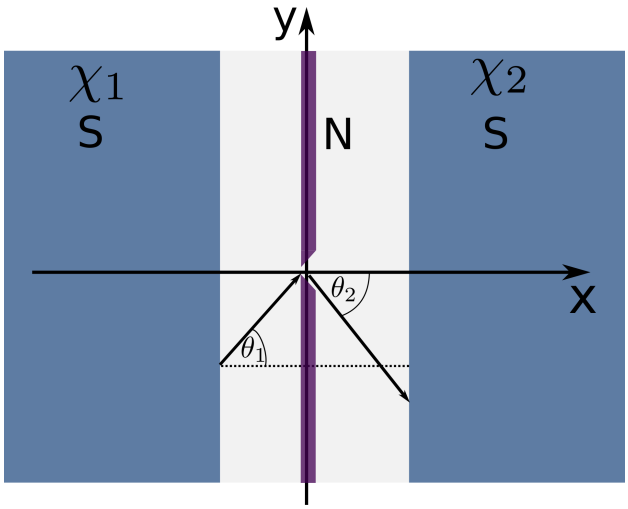

Figure 1.4: *SNS junction with a QPC gate on top. The split is located at* $(x, y) = (0, 0)$ *and the width of the barrier is assumed to be negligible. Each trajectory that contributes has to pass though the origin. The angles* θ_1 *and* θ_2 *parametrize this trajectory.*

With the contribution from side boundary scattering, the total Josephson current is

$$J\left(\chi,\phi\right) = J^{(0)}\left(\chi,\phi\right) + 2J^{(1)}\left(\chi,\phi\right). \tag{1.30}$$

$J^{(0)}$ denotes the part coming from straight trajectories. Since there are two side boundaries, the part describing the scattering, $J^{(1)}$, has an additional factor 2 and reads

$$J^{(1)} = \frac{2ev_F}{\pi\lambda_F L^2}\int\int_{-W/2}^{W/2}\frac{dy_1dy_2}{\left[1+\left(\frac{y_1-y_2}{L}\right)^2\right]^2}\mathcal{J}\left(\chi - \frac{\pi\phi}{2W}\left(2(y_1+y_2) - \frac{(W-2y_1)(W-2y_2)}{W-y_1-y_2}\right)\right) \tag{1.31}$$

This contribution has not been noted in [**?**]. In the case of short and wide junctions, it is sufficient to consider only $J^{(0)}$. For the cases, when $W/L \simeq 1$, it is necessary to sum over all possible edge channels.

1.3 Calculation of QPC current

The quasi classical formalism can even be employed to modified SNS junctions. One can build gates on top of the normal region of the junction in a way that the current cannot pass through the gated regions (see chapter **??**). In the quasi classical picture, this means that the possibilities for trajectories connecting two points at the superconducting interfaces are limited through the geometry of the constriction.
Figure 1.4 shows a sketch of the quantum point contact set-up which will be analysed with the quasi classical formalism. The normal region of the SNS junction is covered by a gate with a small split in the middle. The split is located at $(x, y) = (0, 0)$ so that the sample is symmetric around the origin. The width of the split is in the order of λ_F and can thereby be viewed as an isotropic scattering point with transmission coefficient $\mathcal{T}_0$. Trajectories connecting the two superconducting interfaces have to pass through the QPC. For simplicity, the geometrical width of the barrier is neglected, only straight trajectories are considered, and scattering at side edges is neglected. This modified set-up leads to a different parametrization of the trajectories and therefore to a different

magnetic phase than in eq. (1.15).
With the QPC set-up, all possible trajectories are parametrized by two angles θ_1 and θ_2. θ_1 describes the trajectory before passing through the QPC in the region $-L/2 < x < 0$, and θ_2 after passing through the QPC. The parametrization of the trajectories reads

$$\tan\theta_1 = -\frac{2y_1}{L}, \quad \tan\theta_2 = \frac{2y_2}{L} \tag{1.32}$$

With the gauge from eq. (1.16), the magnetic phase acquired within the sample reads

$$\frac{2\pi}{\Phi_0}\int d\mathbf{l}\cdot\mathbf{A} \;=\; -\frac{\pi B}{\Phi_0}\left(\frac{L}{2}\right)^2\left(-\tan\theta_1+\tan\theta_2\right) = -\frac{\pi\phi(y_1+y_2)}{2W}. \tag{1.33}$$

The total phase difference is the difference of the contribution coming from the magnetic field, eq. (1.33) and the supcondcucting phase difference eq. (1.15). The effective phase for the QPC setup is found to be

$$\tilde{\chi}(y_1,y_2) = \chi - \frac{\pi\phi}{2W}(y_1+y_2). \tag{1.34}$$

One consequence of the additional gate on top of the normal region is the change in the effective phase, resulting in a modified current phase relation $\mathcal{J}(\tilde{\chi}(y_1,y_2))$. Another consequence is a modified expression for the critical current. In the set-up without gates, straight trajectories with a fixed angle θ were considered and summed up to a total contribution. The difference in the QPC set-up is the split in the gate, which is modelled as an isotropic scattering point. The trajectories being summed up in this set-up can be thought to consist of two parts. The first part connects y_1 with the split at $(x,y)=(0,0)$ and is determined by the direction of the trajectory. This explains the Fermi velocity in this part(?). The second part of the current trajectory starts from the origin and connects it with a point at the right interface y_2. Summing up, the critical current in the QPC set-up is

$$I_c^{\mathrm{QPC}}(\phi) \propto \max_\chi \int d\theta_1 v_F \cos^2\theta_1 \int d\theta_f \cos\theta_f \mathcal{J}\left(\tilde{\chi}(\theta_1,\theta_2)\right) \tag{1.35}$$

The QPC is modelled as an isotropic scatterer with transmission probability $\mathcal{T}$. If the transmission is small, $\mathcal{T} << 1$, eq. (1.12) can be used for $\mathcal{J}$. The angles $\theta_{1,2}$ can be rewritten in terms of $y_{1,2}$ by using the parametrization from eq. (1.32), allowing the normalized critical current to be expressed as

$$\frac{I_c(\phi)}{I_c(0)} \;=\; \frac{\mathcal{I}_2(\phi)\mathcal{I}_{3/2}(\phi)}{\mathcal{I}_2(0)\mathcal{I}_{3/2}(0)}, \tag{1.36}$$

where the integrals $\mathcal{I}$ are defined as

$$\mathcal{I}_k(\phi) = \frac{2}{L}\int_{-W/2}^{+W/2} dy \frac{\cos\left(\frac{\pi\phi y}{2W}\right)}{\left[1+\left(\frac{2y}{L}\right)^2\right]^k} \tag{1.37}$$

Numerical evaluation

Evaluating the integral numerically, one finds

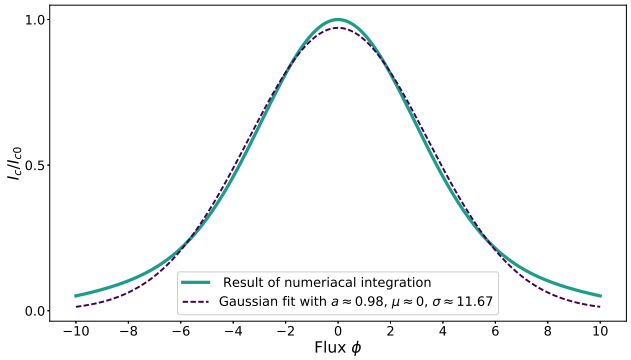

Evaluation in limits

The current can be evaluated in the limit of small flux $\phi \to 0$, and in limit of high fields $\phi \to \infty$. At $\phi = 0$ the cosine term becomes one leading to the simple expression

$$\mathcal{I}_2(0)\mathcal{I}_{3/2}(0) = \frac{2W^2L}{\left(L^2+W^2\right)^{3/2}} + \frac{2W}{\sqrt{L^2+W^2}} \arctan\frac{W}{L} \tag{1.38}$$

$$\equiv \frac{2x^2}{\left(1+x^2\right)^{3/2}} + \frac{2x}{\sqrt{1+x^2}} \arctan x, \tag{1.39}$$

where $x \equiv W/L$. The parabolic asymptotics of the critical current at small ϕ is found by expanding the cosine factors in the numerator:

$$\frac{I_c(\phi)}{I_{c0}} \simeq 1 - \frac{\pi^2\phi^2}{32} f_0(W/L) \tag{1.40}$$

$$f_0(x) = \frac{\sqrt{x^2+1}\log\left(\sqrt{x^2+1}+x\right)}{x^3} - \frac{2}{x(x+(x^2+1)\arctan x)} \tag{1.41}$$

In the opposite limit of high fields, $\phi \to \infty$, the integration in eq. (1.37) is extended over y_1 and y_2 to $\pm\infty$ and obtain

$$\frac{I_c(\phi)}{I_{c0}} = \frac{\pi^{3/2}}{8x} \frac{(1+x^2)^{3/2}}{x+(1+x^2)\arctan x} \left(\frac{\pi\phi}{2x}\right)^{3/2} \exp\left(-\frac{\pi\phi}{2x}\right) \tag{1.42}$$

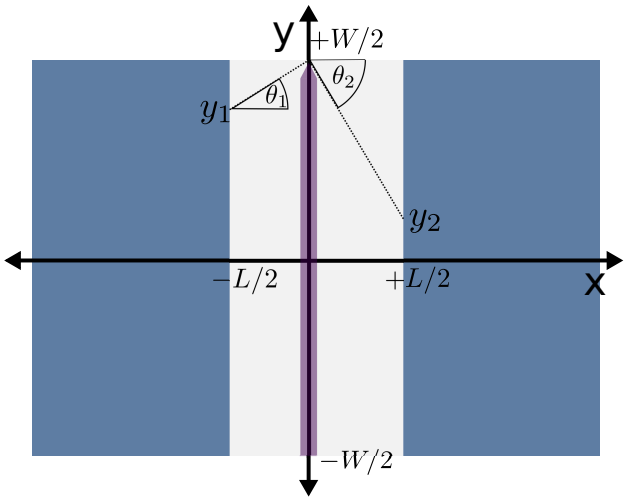

Figure 1.5: *A SNS junction with split at upper edge, $(x, y) = (0, +W/2)$. Similar to the QPC set-up, this constriction is formed in a way that each trajectory has to pass through to contribute to the current.*

1.4 QPC edge current

Additionally to the QPC, two edge channels at $(x, y) = (0, \pm w/2)$ are introduced. The QPC is modelled with the transmission coefficient $\mathcal{T}_q$, and the edge channel with the coefficient $\mathcal{T}_e$. The lattice orientation of the graphene structure may may be either predominantly arm-chair or zigzag. Depending on this orientation, the edge currents may or may not contribute significantly to the total current. The Fraunhofer pattern changes accordingly. The parametrization of an edge trajectory, illustrated in figure **??**, reads

$$\tan\theta_1 = \frac{W - y_1}{L/2}, \quad \tan\theta_2 = -\frac{W - y_2}{L/2}. \tag{1.43}$$

Similar to the QPC contribution, the magnetic phase gain along the trajectory is calculated. For the upper edge, the result is

$$\begin{aligned}
\frac{2\pi}{\phi_0}\int d\mathbf{l}\cdot\mathbf{A} &= \frac{2\pi}{\phi_0}\left(\int A_y(x)|d\mathbf{l}||\mathbf{e_y}|\sin\theta_1 + \int A_y(x)|d\mathbf{l}||\mathbf{e_y}|\sin\theta_2\right) && (1.44)\\
&= -\frac{2\pi B}{\phi_0}\left(\int_{-L/2}^{0} x dx\tan\theta_1 + \int_0^{L/2} x dx\tan\theta_2\right) && (1.45)\\
&= -\frac{\pi B}{\phi_0}\frac{L}{2}\left(-\tan\theta_1 + \tan\theta_2\right) && (1.46)\\
&= -\frac{\pi B}{\phi_0}\frac{L}{2}\left(-2W + (y_1 + y_2)\right) && (1.47)\\
&= \pi\Phi - \frac{\pi\Phi}{2W}(y_1 + y_2), && (1.48)
\end{aligned}$$

where

$$\Phi = \frac{\phi}{\phi_0}, \quad \phi = BWL \tag{1.49}$$

has been used. Together with the contribution from the set-up without any constriction from eq. (1.15), the total phase for the edge transmission is added up to

$$\tilde{\chi}(y_1, y_2) = \chi - \frac{3\pi\Phi}{2\phi_0}(y_1 + y_2) + \pi\Phi. \tag{1.50}$$

This is the effective phase $\tilde{\chi}(y_1, y_2)$ for the upper edge. Analogously, the phase for the lower edge can be constructed with a simple sign change in the parametrization in eq. (1.43), leading to

$$\tilde{\chi}(y_1, y_2) = \chi + \frac{3\pi\Phi}{2\phi_0}(y_1 + y_2) - \pi\Phi \tag{1.51}$$

The Josephson relation for the edge contribution has the modified phase from eq. (1.51). The result for the QPC in the limit in high fields, eq. (**??**), has a transmission coefficient $\mathcal{T} = 1$. For easier comparison with the edge channel contribution, this is rewritten into the following form

$$I_c^{\mathrm{QPC}} = \mathcal{T}_q F(W/L) \tag{1.52}$$

, where the function $F(W/L)$ represents the result from eq. (1.42). The integrals for the upper edge can be written in a similar way:

$$I_c^e = \mathcal{T}_e \sin\left(\chi_0 - \pi\Phi\right) \int_0^\infty d\tilde{y}_1 \int_0^\infty d\tilde{y}_2 \frac{\cos\left(\frac{3\pi\Phi\tilde{y}_1}{2W}\right)}{\left(1 + \left(\frac{2\tilde{y}_1}{L}\right)^2\right)^2} \frac{\cos\left(\frac{3\pi\Phi\tilde{y}_2}{2W}\right)}{\left(1 + \left(\frac{2\tilde{y}_1}{L}\right)^2\right)^{3/2}} \tag{1.53}$$

$$= \mathcal{T}_e \sin\left(\chi_0 - \pi\Phi\right) \frac{F(W/L)}{4}, \tag{1.54}$$

where

$$\tilde{y}_{1/2} = W/2 - y_{1/2} \tag{1.55}$$

The total critical current though the junction is proportional to the sum of the individual contributions

$$\frac{I_c\left(\phi\right)}{I_{c0}} = \max_\chi \left\{ \mathcal{T}_q \sin\chi + \frac{\mathcal{T}_e}{4} \sin\left(\chi - \pi\phi\right) + \frac{\mathcal{T}_e}{4} \sin\left(\chi + \pi\phi\right) \right\} / \left(\mathcal{T}_q + \mathcal{T}_e/2\right) \tag{1.56}$$

$$= \frac{\mathcal{T}_q/\mathcal{T}_e + \cos\left(\pi\phi\right)/2}{\mathcal{T}_q/\mathcal{T}_e + 1/2} \tag{1.57}$$

The result of eq. (1.57) is plotted in figure 1.6. Figure 1.7 shows a plot of the ratio from eq. (1.57) multiplied with a gaussian curve.

TODOs:
make plot colors uniform
add figure captions
check plots for edge current −¿ cbar seems wrong

1.5 Barrier with finite split width - Transition to QPC setup

The QPC setup and the SNS setup without barriers can be linked conceptually by investigating an hourglass-shaped setup. This setup constricts the trajectories through a split with a finite width w_s and is visualized in figure (1.8). When considering only straight trajectories, this split width models the transition to the QPC in the limit of $w_s \to 0$. The difference to the QPC is simply the

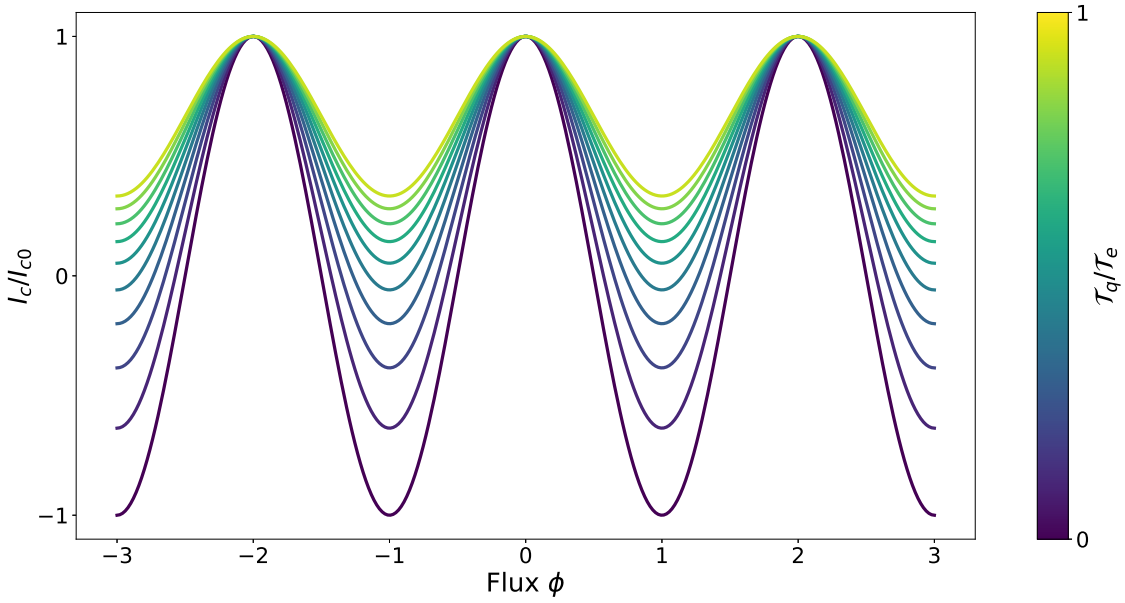

Figure 1.6: *Another figure caption. Whatever.*

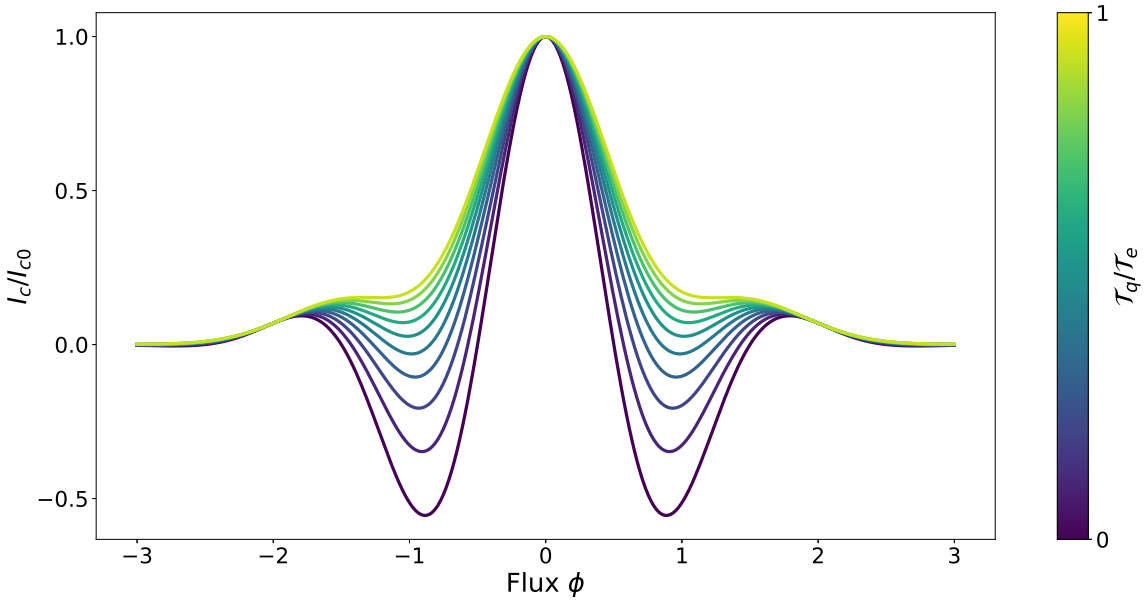

Figure 1.7: *Some figure.*

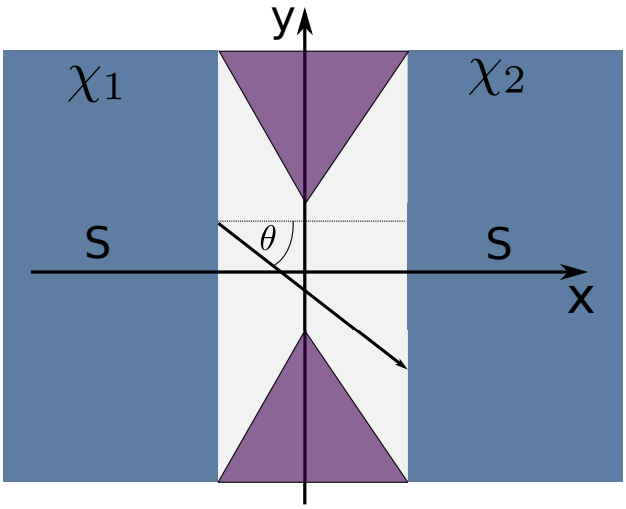

Figure 1.8: *Hourglass setup*

parametrization of the angles: with a finite w_s, trajectories are parametrized by only one angle θ, the direction does not change after passing the split. When w_s is small enough, like in the QPC case, two independent trajectories are considered with two parametrization angles θ_1 and θ_2. This setup is particularly interesting because the impact of asymmetry in the junction can be studied. When relocating the split by for example moving it along the x-axis, the possible trajectories are limited. As a consequence, the Fraunhofer pattern changes.

2 Conclusion and Outlook

Bibliography

[1] Edward McCann and Mikito Koshino. The electronic properties of bilayer graphene. may 2012.

[2] A. H. Castro Neto et al. The electronic properties of graphene. *Reviews of Modern Physics*, 81(1):109–162, jan 2009.

[3] M.S. Dresselhaus, G. Dresselhaus and R. Saito. Physics of carbon nanotubes. *Carbon*, 33(7): 883–891, jan 1995.

[4] J. W. McClure. Band Structure of Graphite and de Haas-van Alphen Effect. *Physical Review*, 108(3):612–618, nov 1957.

[5] J. W. McClure. Theory of Diamagnetism of Graphite. *Physical Review*, 119(2):606–613, jul 1960.